Mon. Not. R. Astron. Soc. **386,** 1907–1921 (2008) doi:10.1111/j.1365-2966.2008.13197.x

The SCUBA Half Degree Extragalactic Survey (SHADES) – IX. The environment, mass and redshift dependence of star formation

S. Serjeant,[1] S. Dye,[2] A. Mortier,[3] J. Peacock,[3] E. Egami,[4] M. Cirasuolo,[3] G. Rieke,[4] C. Borys,[5] S. Chapman,[6] D. Clements,[7] K. Coppin,[8] J. Dunlop,[3] S. Eales,[2] D. Farrah,[9] M. Halpern,[10] P. Mauskopf,[2] A. Pope,†[10,11] M. Rowan-Robinson,[7] D. Scott,[10] I. Smail[8] and M. Vaccari[12]

[1]*Department of Physics and Astronomy, The Open University, Milton Keynes MK7 6AA*
[2]*School of Physics & Astronomy, Cardiff University, Queens Buildings, The Parade, Cardiff CF24 3AA*
[3]*Institute for Astronomy, The University of Edinburgh, Royal Observatory, Blackford Hill, Edinburgh EH9 3HJ*
[4]*Department of Astronomy, University of Arizona, 933 N Cherry Avenue, Rm. N204, Tucson, AZ 85721-0065, USA*
[5]*Department of Astronomy & Astrophysics, University of Toronto, 60 St. George Street, Toronto, ON M5S 3H4, Canada*
[6]*Institute of Astronomy, University of Cambridge, Madingley Road, Cambridge CB3 0HA*
[7]*Astrophysics Group, Imperial College London, Blackett Laboratory, Prince Consort Road, London SW7 2AZ*
[8]*Institute for Computational Cosmology, Durham University, South Road, Durham DH1 3LE*
[9]*106 Space Sciences Building, Cornell University, Ithaca, NY 14853, USA*
[10]*Department of Physics & Astronomy, University of British Columbia, 6224 Agricultural Road, Vancouver, BC V6T 1Z1, Canada*
[11]*National Optical Astronomy Observatory, 950 North Cherry Avenue, Tucson, AZ 85719, USA*
[12]*Department of Astronomy, University of Padova, vic. Osservatorio 2, 35122 Padova - I, Italy*

Accepted 2008 March 5. Received 2008 March 5; in original form 2007 December 21

ABSTRACT

We present a comparison between the SCUBA (Submillimetre Common User Bolometer Array) Half Degree Extragalactic Survey (SHADES) at 450 and 850 μm in the Lockman Hole East with a deep *Spitzer* Space Telescope survey at 3.6–24 μm conducted in guaranteed time. Using stacking analyses we demonstrate a striking correspondence between the galaxies contributing the submm extragalactic background light, with those likely to dominate the backgrounds at *Spitzer* wavelengths. Using a combination *BRIzK* plus *Spitzer* photometric redshifts, we show that at least a third of the *Spitzer*-identified submm galaxies at $1 < z < 1.5$ appear to reside in overdensities when the density field is smoothed at 0.5–2 Mpc comoving diameters, supporting the high-redshift reversal of the local star formation–galaxy density relation. We derive the dust-shrouded cosmic star formation history of galaxies as a function of assembled stellar masses. For model stellar masses $<10^{11}\,\mathrm{M}_{\odot}$, this peaks at lower redshifts than the ostensible $z \sim 2.2$ maximum for submm point sources, adding to the growing consensus for 'downsizing' in star formation. Our surveys are also consistent with 'downsizing' in mass assembly. Both the mean star formation rates $\langle \mathrm{d}M_*/\mathrm{d}t \rangle$ and specific star formation rates $\langle (1/M_*)\,\mathrm{d}\,M_*/\mathrm{d}\,t \rangle$ are in striking disagreement with some semi-analytic predictions from the Millenium Simulation. The discrepancy could either be resolved with a top-heavy initial mass function, or a significant component of the submm flux heated by the interstellar radiation field.

Key words: galaxies: evolution – galaxies: formation – galaxies: starburst – cosmology: observations – infrared: galaxies – submillimetre.

1 INTRODUCTION

The SCUBA (Submillimetre Common User Bolometer Array) Half Degree Extragalactic Survey (SHADES; Mortier et al. 2005; Coppin et al. 2006) is a long-term submm survey conducted at the James Clerk Maxwell Telescope (JCMT) from 2003 to 2005. A key goal of SHADES has been to determine whether submm galaxies are the likely progenitors of giant ellipticals. The clustering of submm galaxies is a strong discriminant of competing models (van Kampen et al. 2005), and measurement of the angular correlation function of submm galaxies in broad $\Delta z \simeq 0.5$ redshift shells is one of the

†*Spitzer* Fellow.

principal experimental aims of SHADES. In this paper we will take a different approach to the problem, by estimating the matter overdensities in which submm galaxies reside via the assembled stellar masses in the submm galaxy environments. The SHADES survey was conducted in two fields, each with abundant multiwavelength supporting survey data. The $\sim$0.1 deg^2 surveyed by SHADES in the Lockman Hole East field, in particular, has some of the best *Spitzer* Space Telescope data of any contiguous field over hundreds of square arcminutes. The comparison between SHADES and this *Spitzer* data, which was taken in *Spitzer* guaranteed time, forms the basis of our constraints on the submm galaxy environments, and allows us important new insights on the submm extragalactic background light.

The galaxies that dominate the extragalactic background light at any given redshift are necessarily the same as those which dominate the comoving volume-averaged luminosity density at that redshift (e.g. Peacock 1999). The favourable *K*-corrections in the submm make the submm extragalactic background light sensitive to the cosmic star formation history throughout most of the history of the Universe. Resolved submm point sources from blank field surveys (i.e. those at the few mJy level) contribute a few tens of per cent to the 850-μm extragalactic background, but cannot account for all of it (Barger et al. 1998; Hughes et al. 1998; Barger, Cowie & Sanders 1999; Blain et al. 1999; Eales et al. 2000; Cowie, Barger & Kneib 2002; Scott et al. 2002; Smail et al. 2002; Scott, Dunlop & Serjeant 2006). At 350–450 μm there are very few reliably detected resolved point sources (e.g. Scott et al. 2002; Khan et al. 2005, 2007), and those that have been detected are far from accounting for the majority of the 450-μm extragalactic background light. However, 850-μm-selected galaxies can be readily detected at 350–450 μm and can account for a minority of the 350–450 μm background (e.g. Chapman et al. 2005; Khan et al. 2005, 2007; Kovács et al. 2006; Coppin et al. 2008).

This situation, particularly at 450 μm, will change with the advent of the SCUBA-2 camera on the JCMT. In the meantime, attention has focused on stacking analyses. Instead of aiming to detect individual resolved galaxies, this approach seeks to detect the average signal from a population. This has met with some success. Peacock et al. (2000) found a $\sim 3\sigma$ signal at 850 μm from the Lyman-break population in the *Hubble Deep Field*-North. The submm:UV flux ratio suggested an obscuration very different to that of the submm point source population, and there were hints of a flat redshift distribution at $z > 1$ in these faint submm-emitting galaxies. Further stacking analyses of extremely red galaxies (e.g. Webb et al. 2004; Takagi et al. 2007) found them to contribute a significant minority of the obscured star formation history. A submm stacking analysis of near-infrared (IR) and mid-IR selected galaxies from the 5×5 arcmin^2 *Spitzer* Early Release Observations (Serjeant et al. 2004) found that *Spitzer* 5.8- and 8-μm populations could account for around a quarter of the 850-μm extragalactic background light, and the majority of the 450-μm background, albeit in a small sample. The sample size was not large enough in this study to distinguish the stacked signal from low-redshift red dusty galaxies, and that from high-redshift galaxies.

To constrain the redshift ranges responsible for the submm extragalactic background light, larger samples were needed. Wang, Cowie & Barger (2006) and Dye et al. (2006) both made stacking analyses of *Spitzer*-selected galaxies, though in the former case it was combined with *H*-band selection. Both groups found that *Spitzer* galaxies contribute significantly to the submm extragalactic background light. However, the redshift ranges responsible in these surveys differed, with Wang et al. finding the $z < 1$ population dominating (their fig. 12), while Dye et al. found $z > 1$ the more important (their fig. 6) though with slightly larger errors. One possible explanation for this difference is cosmic variance; the wide-area SHADES would be ideal to resolve this controversy. Another possibility is the effect of redshifted PAH features in the Dye et al. analysis, which would not be present in the $\leqslant$ 3.6-μm Wang et al. analysis.

In this paper we extend these results to a deeper *Spitzer* catalogue, and a wider area submm survey. In a confusion-limited submm survey, the stacking signal-to-noise ratio (S/N) is roughly proportional to the square root of the number of submm beams, and since SHADES is the widest area contiguous submm survey to a depth approaching the effective point source extraction limit (Scott et al. 2002), this is the best opportunity to date to examine the submm stacking signal of *Spitzer* galaxies.

This paper is the ninth in the SHADES series of papers. Paper I (Mortier et al. 2005) presented the survey design, motivation and data analysis. Paper II (Coppin et al. 2006) presented further data analysis, the source counts, the catalogues and the maps. Paper III (Ivison et al. 2007) gave the radio and *Spitzer* 24-μm identifications of the submm galaxies in SHADES. Paper IV (Aretxaga et al. 2007) made photometric redshift estimates of the SHADES catalogue galaxies using the far-IR to radio spectral energy distributions (SEDs). Paper V (Takagi et al. 2007) examined the submm properties of near-IR galaxies in the SHADES survey data in the Subaru–*XMM* Deep Field. Paper VI (Coppin et al. 2008) presented the results of 350-μm observations of a subset of SHADES sources. Paper VII (Dye et al. 2008) made fits to the SEDs of the SHADES galaxies in the Lockman Hole and Paper VIII (Clements et al. 2008) performed a similar analysis for the SHADES galaxies in the Subaru–*XMM* Deep Field. Paper X (van Kampen et al., in preparation) measures the clustering of the submm galaxies in the SHADES survey. A further series of papers will concern the 1.1-mm data taken to supplement the SHADES survey with the AzTEC instrument on the JCMT.

This paper is structured as follows. The *Spitzer* and submm data are summarized briefly in Section 2. Section 3 describes our methodology and results. We discuss the context of our results in Section 4, and we draw conclusions in Section 5. Throughout the paper we assume a 'concordance' cosmology, with density parameters $\Omega_{\rm M} = 0.3$ and $\Omega_\Lambda = 0.7$ and a Hubble constant of $H_0 = 72\,{\rm km\,s^{-1}\,Mpc^{-1}}$.

2 DATA ACQUISITION

The submm data were taken from 2003 to 2005 at the JCMT with the SCUBA camera, in submm opacities of $0.265 < \tau_{850\,\mu{\rm m}} < 0.283$ and $1.41 < \tau_{450\,\mu{\rm m}} < 1.52$, i.e. JCMT weather bands 2–3. Chopping/nodding was performed at position angles of 0° and 90°, with chop throws of 30, 44 and 68 arcsec, though at the centre of the map only the 30 arcsec/90° combination was used (Scott et al. 2002). The submm data acquisition, calibration, reduction and analysis are described in full in Mortier et al. (2005). A noise-weighted point source filtering was made on the maps, and the separate chop/nod images were combined optimally (Serjeant et al. 2003a, Mortier et al. 2006). Note that the SCUBA 450-μm absolute flux calibration is typically uncertain to $\sim$30 per cent. The maps from this analysis are used in this paper. Three further parallel data reduction efforts are described in Coppin et al. (2006), and 850-μm maps from some of these reductions have been used to test the robustness of the results presented in this paper. The 450-μm maps used in this paper are from the SHADES data reduction described as the 'primary' reduction in Mortier et al. (2005), and analysis 'B' in the later Coppin

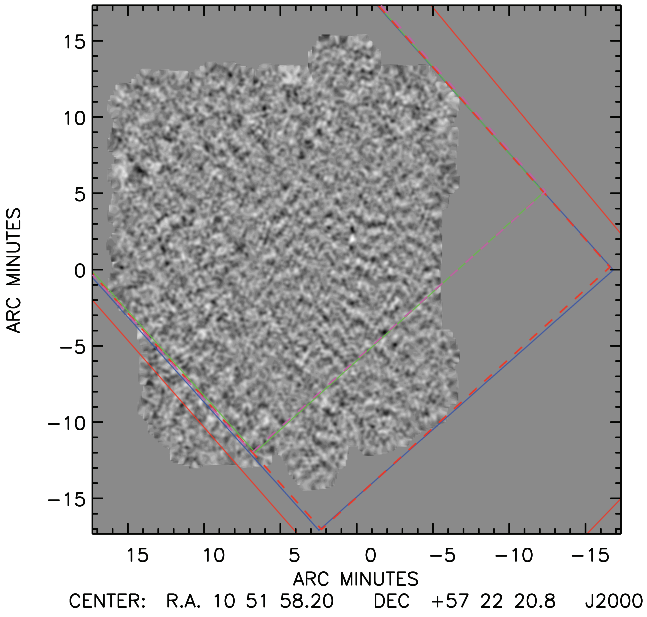

Figure 1. The SHADES 850-μm map with point sources subtracted, used for stacking analyses in this paper (grey-scale). Also plotted is the coverage of the *Spitzer* 24-μm data (solid red line), the 3.6-μm data (solid blue line), 4.5-μm data (solid green line), 5.8-μm data (dashed red line) and 8-μm data (dashed magenta line). Note the availability of *Spitzer* data over most of the SHADES area.

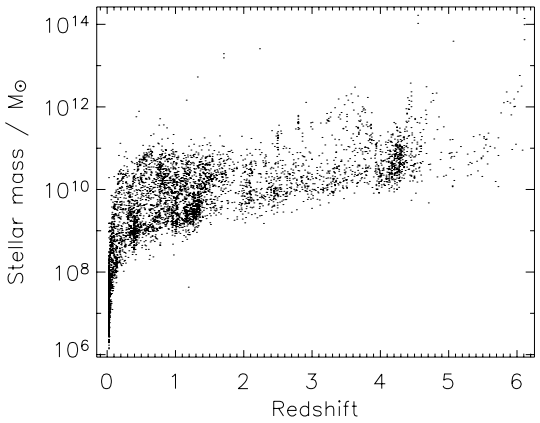

Figure 2. Model stellar mass estimates of *Spitzer* galaxies discussed in the text, versus photometric redshifts from Dye et al. (2008, SHADES Paper VII). Note that the model stellar masses above $z = 0.5$ depend only weakly on photometric redshift.

et al. (2006). These maps have the lowest noise of the available 450-μm maps, and have short time-scale opacity variations modelled using the water vapour meter. No reliable 450-μm point sources are detected in SHADES, though this is not to say that one cannot find point source candidates in the maps. A cross-comparison of the four reductions found very few overlaps between the candidate source lists; this demonstrated that the 450-μm opacity during the SHADES runs (see appendix A of Coppin et al. 2006), and the stability of the opacity, were not suited to reliable point source extraction. We will show that this does not preclude statistical constraints on the 450-μm-emitting populations. The 850-μm maps of the four data reduction methods are in excellent agreement (Coppin et al. 2006), and the SHADES point source list is derived from the consensus of the four analyses.

The *Spitzer* data were taken in guaranteed time, using the IRAC and MIPS instruments (Fazio et al. 2004; Rieke et al. 2004). As shown in Fig. 1, most of the SHADES survey area in the Lockman Hole East is covered at 3.6 μm (4.47 μJy, 3σ), 4.5 μm (4.54 μJy, 3σ), 5.8 μm (20.9 μJy, 3σ), 8 μm (12.5 μJy, 3.2σ) and 24 μm (38 μJy, 4σ). We only use *Spitzer* IRAC sources detected in at least two *Spitzer* bands. The area was also mapped at 70 and 160 μm, and the comparison between this data and SHADES will be the subject of a future paper (Egami et al., in preparation). Most of the SHADES Lockman field was also covered by a deep 15-μm survey with the CAM instrument on the *Infrared Space Observatory* (*ISO*), further details of which can be found in Elbaz et al. (1999) and Rodighiero et al. (2004). We select galaxies with 15-μm flux densities above 100 μJy for this paper. The Subaru–*XMM* Deep Field was also observed by SHADES, and has *Spitzer* data from the SWIRE survey (Lonsdale et al. 2004), but since these data are significantly shallower than the Lockman data we do not consider them here.

BRIz imaging was obtained from the SUPRIMECAM instrument on the Subaru telescope to 5σ point source depths of 26.8, 25.8, 25.7 and 25.0 in B, R, I and z, respectively (3-arcsec diameter AB magnitudes). *K*-band photometry was obtained from the UKIRT Deep Infrared Sky Survey (UKIDSS; Lawrence et al. 2007) to a point source sensitivity of 22.9 (5σ AB magnitude). Further details are in Dye et al. (2008, Paper VII).

3 METHODOLOGY AND RESULTS

3.1 Photometric redshift estimates

We use the *Spitzer* galaxy photometric redshift catalogue of Dye et al. (2008). This catalogue is derived using the HYPER-Z code (Bolzonella, Miralles & Pelló 2000) applied to the nine-band optical-IRAC photometric catalogue. Further details of the SED templates are found in Dye et al. (2008). In Fig. 2 we show the model stellar masses (derived below) as a function of the photometric redshifts. Note that redshift aliasing can scatter galaxies to erroneously high redshifts (and hence to high masses), and there are plausible examples of this in Fig. 2. We have opted not to impose any arbitrary cuts in the photometric redshift catalogue to remove these outliers, and instead leave this to the discretion of the reader. Redshift aliasing and consequent erroneously high stellar masses in a small subset would not alter the statistical conclusions of this paper.

Dye et al. (2008) also uses optical and *Spitzer* photometery to derive photometric redshift estimates for the SHADES galaxies themselves, and comparisons with other redshift estimators can be found in Aretxaga et al. (2007), Clements et al. (2008) and Dye et al. (2008). We will use the Dye et al. (2008) determinations in this paper. The main disadvantage of the photometric redshifts in the Lockman Hole is the lack of spectroscopic training sets, though a comparison of the Dye et al. photometric redshifts of submm-selected galaxies with their spectroscopic redshifts, and between independent photometric redshift determinations (their figs 3 and 4) shows the photometric redshifts are accurate to $|\Delta z|/(1+z) \simeq 0.09$ consistent with other studies (e.g. Chapman et al. 2005; Pope et al. 2006). This is more than sufficient for our purposes.

3.2 Mass estimates of *Spitzer* galaxies

The 3.6- and 4.5-μm IRAC bands are dominated by the redshifted light from old stellar populations, and are therefore useful

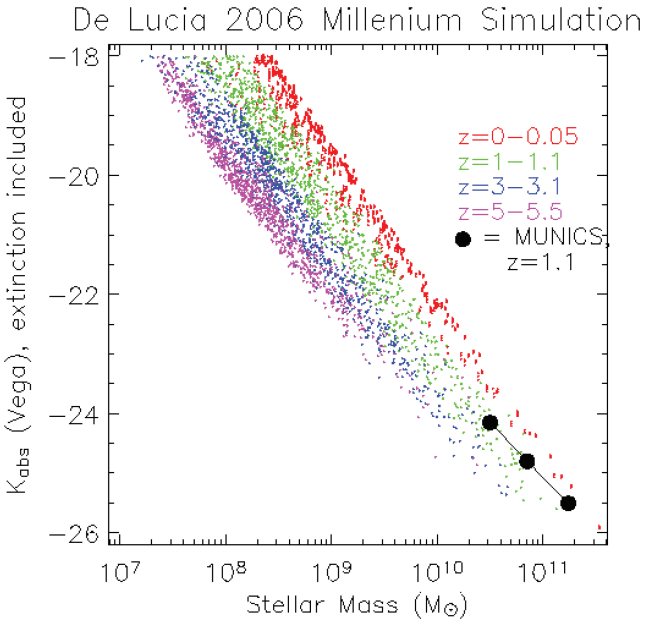

Figure 3. Correlation between model stellar mass and absolute K magnitude predicted using the Millenium Simulation by de Lucia et al. (2006) for several redshift shells. Also plotted are the data from the MUNICS survey (Drory et al. 2004). Note the small dispersion and the clear redshift dependence.

estimators of the assembled stellar masses. The K-corrections are also simple at these wavelengths, since it samples the Rayleigh–Jeans tail of the stellar photospheric emission. We use the model SEDs from Dye et al. (2008) to obtain rest-frame K-band monochromatic luminosities; the results are insensitive to the assumed SED.

There is no accepted conversion between rest-frame K-band luminosity and stellar mass, as a function of redshift. Our aim is to compare our results with the de Lucia et al. (2006) Millenium Simulation, and one can only do this self-consistently by adopting a conversion consistent with that simulation. Therefore, we adopt an empirical conversion based on these simulations, based on fits to the simulated data in Fig. 3. This conversion is consistent with the observed luminosity-dependent evolution in K-band stellar mass-to-light ratios in the MUNICS survey (Drory et al. 2004). Our conversion is

$$\log_{10} M_* = a(z) + b(z)\, K_{\rm abs,AB}, \quad (1)$$

where the values of a and b are interpolated from the best-fitting values tabulated in Table 1.

In calculating the matter overdensities, we add a dark matter contribution following the total mass estimates from gravitational lenses by Ferreras, Saha & Williams (2005), who found that the total mass scales as the stellar mass to the 1.2 power, with total mass equalling stellar mass at $3.18 \times 10^9\,{\rm M}_\odot$. Below this mass we make no correction for dark matter contribution. Our results are not sensitive to the dark matter assumptions.

3.3 The density field around submm galaxies

As shown in Blake et al. (2006), the SHADES survey does not have enough sources or field galaxy redshifts to accurately determine the galaxy–SHADES cross-correlation function. We therefore used an alternative estimator which is essentially a stack of the 3.6-μm *Spitzer* data at the positions of the SHADES sources. Using *Spitzer* galaxy mass estimates discussed above, we created projected mass density maps in broad redshift bins, and smoothed each map with a top-hat circular kernel with 0.5–2 comoving Mpc diameters at the central redshift of the bin. We then compared the projected matter density at the positions of the SHADES galaxies with the histogram of matter density for the map as a whole, using methods similar to established techniques for stacking analyses (see e.g. Section 3.4). We omitted SHADES galaxies lying in regions with zero density (neither 3.6-μm identification nor sufficiently close neighbours) and also restricted the comparison to the non-zero density regions of the map as a whole.

Table 1. Best-fitting values for the conversion between K-band AB absolute magnitude and stellar mass using equation (1), from the de Lucia (2005) Millenium Simulation. The top row gives the redshift, and the other rows give the fitted parameters in a narrow redshift bin centred on that redshift.

z	0.025	1.05	2.05	3.05	4.1	5.25
a	2.007	1.457	1.156	0.8193	0.3064	0.5831
b	−0.3944	−0.4010	−0.4058	−0.4178	−0.4373	−0.4190

This comparison is shown in Figs 4 and 5 where the percentile of the submm galaxies' environment is plotted against redshift. In the 0.5-Mpc smoothing case, the submm galaxies in the lower redshift bin lie in the top 10–20 percentile of the matter density distribution. However, the small smoothing kernel leaves large regions of the map with no density field data, so the sample of submm galaxies is small. In the 2-Mpc smoothing case, the sample size is more than doubled; only five galaxies are excluded in the lowest redshift bin. The submm galaxies appear to lie in a wide range of environments, but around a third of the submm galaxies at $1 < z < 1.5$ lie in the top 15 percentile of the density distribution.

We performed a similar calculation for 3.6-μm-selected galaxies, which are plotted as small dots in Figs 4 and 5. These appear to have a more uniform distribution in the lower redshift bin than the submm galaxies. We compared the submm galaxy and 3.6-μm-selected

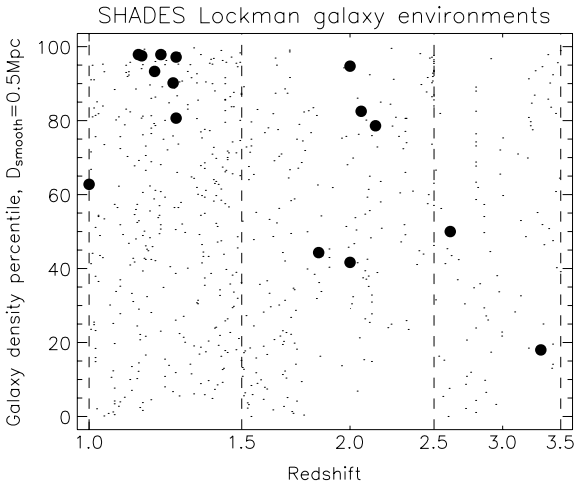

Figure 4. Density distribution percentiles for submm galaxies (large symbols), compared with that of 3.6-μm-selected galaxies (dots). The matter density distribution estimated from *Spitzer* 3.6-μm imaging in broad redshift bins (indicated by dashed lines) was smoothed with a 0.5 comoving Mpc diameter top hat kernel as discussed in the text. Regions with zero estimated density were excluded from this test. Note that submm galaxies sample the highest 10–20 percentiles of this matter density distribution at lower redshifts.

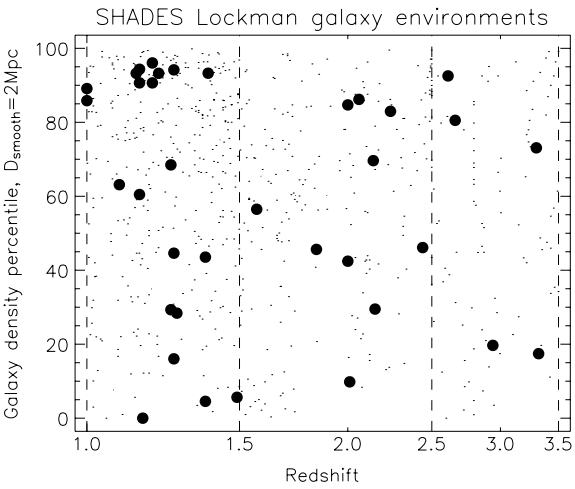

Figure 5. Density distribution percentiles for submm galaxies, compared with that of 3.6-μm-selected galaxies (dots). The matter density distribution estimated from *Spitzer* 3.6-μm imaging in broad redshift bins (indicated by dashed lines) was smoothed with a 2 comoving Mpc diameter top hat kernel as discussed in the text. Regions with zero estimated density were excluded from this test. Note that around half of the submm galaxies in the lower redshift bin sample the highest 10–20 percentiles of this matter density distribution, when smoothed to this scale. The larger smoothing width reduces the area with no density field data, so the sample of submm galaxies is larger.

populations in the $1 < z < 1.5$ bin using a Kolmogorov–Smirnoff test. In the 2-Mpc smoothing case the difference is only marginally significant (32 per cent probability that the distributions are the same), but in the 0.5-Mpc case the distributions are clearly different (0.2 per cent probability that the distributions are the same). Note that in making this comparison, we have subtly changed the question we are asking. We wish to know if submm galaxies lie in richer environments than average, but this average can be taken as a volume average or as a per galaxy average. The raw percentiles address the former, and the submm-*Spitzer* comparison addresses the latter.

3.4 The submm emission of *3–24* μm *Spitzer* galaxies

In Serjeant et al. (2004), the regions of the map near submm point sources were simply excluded from the analysis. This runs the risk of removing the submm signal from companions to the submm point source. Here, point sources detected in the combined point-source-filtered 850-μm map with significance levels of $\geqslant 3.5\sigma$ were subtracted from the original chop/nod images, which were then filtered with the chopped/nodded point source kernels, and the maps were optimally combined to create a residual 850-μm image. This is the same as the procedure adopted by Dye et al. (2006), and this is the threshold used for the submm point source catalogue in Coppin et al. (2006). (We will show in Figs 6 and 7 that our results are not sensitive to this threshold.) There is evidence that the submm point source population has different *Spitzer*:submm flux ratios than the *Spitzer*-selected population (Serjeant et al. 2004), so it is important to remove the point source population before stacking. No reliable 450-μm point sources are detected, so the point-source-filtered maps at 450 μm are used without modification. Our methodology differs from that of Wang et al. (2006), in which submm point sources were left in the map.

The submm point spread function sums to exactly zero, because of the negative sidelobes from the chopping and nodding. Therefore, there is no risk of overestimating the submm flux of a given *Spitzer* galaxy by also counting its neighbours (Peacock et al. 2000; Serjeant et al. 2004). This is because the expectation value of the submm flux from (unclustered) neighbouring galaxies equals that of the map, which is exactly zero by virtue of the zero-sum point spread function. The effect of the clustering of the *Spitzer* population is estimated in Section 3.6.

We can therefore calculate the mean submm flux of *Spitzer* galaxies by averaging the measurements at the positions of *Spitzer* galaxies in the submm maps, even if there is >1 *Spitzer* galaxy per submm beam. The difficulty in extracting 450-μm point sources (Section 2) raises the possibility of non-Gaussian features in the maps contributing to the signal. Such non-Gaussian features could be caused by, for example, imperfect sky subtraction or imperfect correction for atmospheric opacity; the sky is many orders of magnitude brighter than the extragalactic signal (e.g. Serjeant et al. 2003a). However, by the Central Limit Theorem, the probability distribution of the *mean* of a sample is approximately Gaussian with a variance σ^2/n where σ^2 is the variance of the underlying distribution being sampled; the distribution of the mean is increasingly Gaussian for larger samples and for more Gaussian-like underlying distributions. Here, the underlying distribution is well approximated as Gaussians (e.g. Mortier et al. 2005), and many thousands of samplings are taken from the underlying distribution. We are therefore confident that the mean flux levels of stacked populations are Gaussian distributed.

The mean flux level has the advantage of being physically interpretable, but it is not necessarily the most efficient detection statistic of a stacked signal. The Kolmogorov–Smirnoff test has been widely used to test whether the distribution of submm fluxes at the positions of interest is a random sampling from the map as a whole (e.g. Serjeant et al. 2004; Dye et al. 2006). This test is asymptotically distribution free, and is therefore insensitive to non-Gaussian features in the underlying maps. Furthermore, a comparison with a control sample (such as randomized submm source positions) is intrinsic to the test, since it compares the flux distribution of the map as a whole with the map fluxes at the positions of interest. It is also possible to translate the Kolmogorov–Smirnoff significance level into an equivalent number of σ of a Gaussian distribution, by inverting $P_{\rm KS} = 0.5\,{\rm erf}(\sigma/\sqrt{2}) + 0.5$.

Some authors have advocated the use of the error-weighted mean fluxes, rather than the unweighted mean stacked fluxes (e.g. Dye et al. 2006). In Serjeant et al. (2004) it was argued that it was not obvious that the Central Limit Theorem would apply to these weighted quantities. However, Dye et al. (2006) tested their weighted means and found them to be only subtly biased. The large area of the SHADES maps may provide an advantage: provided the field of view is sufficiently large, and provided the noise level is sufficiently uniform, the zero-sum point spread function of each individual source will still produce a zero net contribution on average to the S/N and S/N^2 images, as well as to the flux image S. In this paper we will make error-weighted co-added submm postage stamps of the sources to be stacked. We will show that our error-weighted mean fluxes show no evidence for a systematic shift relative to the unweighted mean fluxes.

We applied the methodology of Serjeant et al. (2004) to test whether the submm fluxes at the positions of *Spitzer*/*ISO* galaxies were representative of the submm map as a whole, or whether there is on average positive flux at the *Spitzer*/*ISO* galaxy positions. We excluded regions of the 850-μm map with noise levels above 5 mJy, and regions of the 450-μm map with noise levels above 20 mJy,

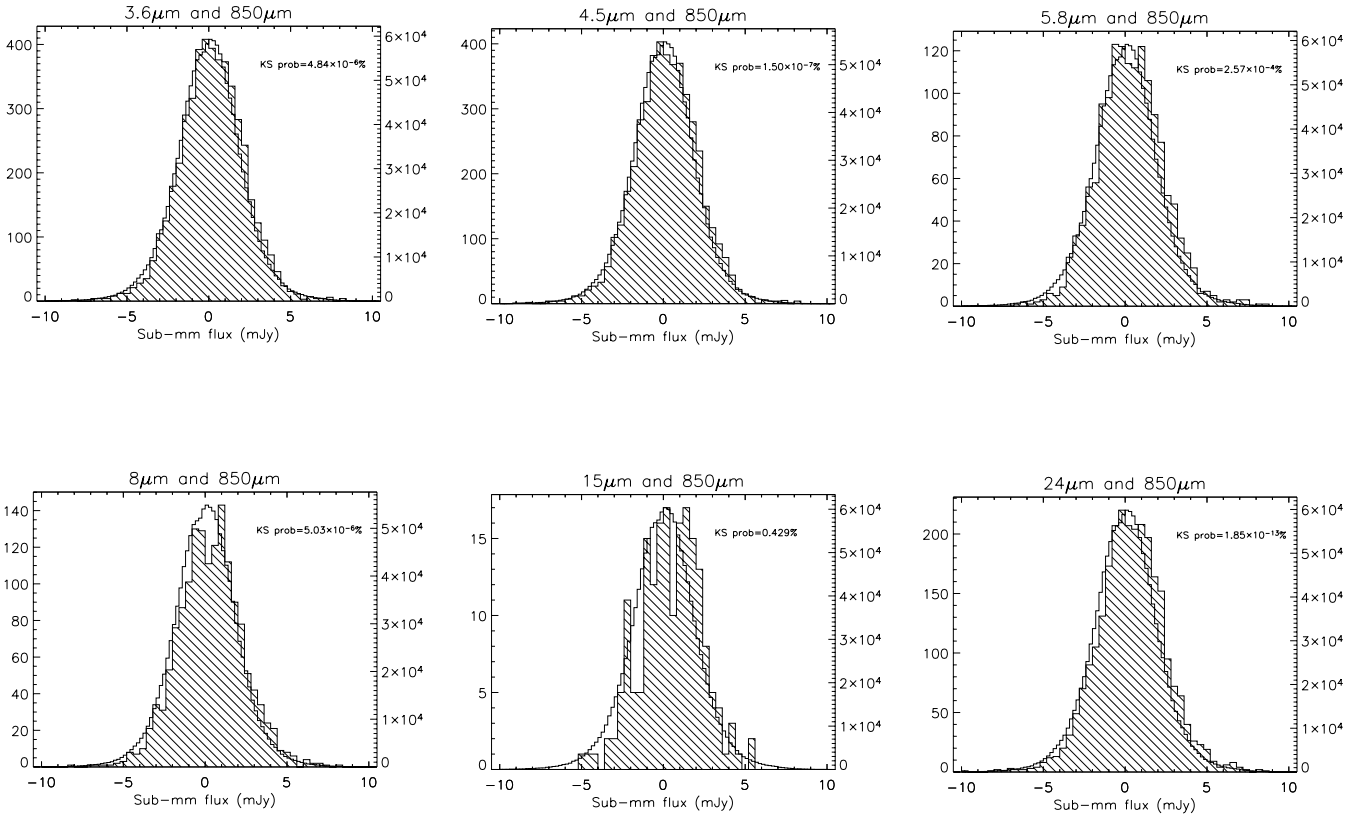

Figure 6. Histograms of 850-μm flux in the SHADES Lockman map as a whole (unhatched bars) compared to the 850-μm fluxes at the positions of the *Spitzer*/*ISO* galaxies selected at the indicated wavelengths (hatched bars). The left-hand side vertical scales show the numbers for the hatched histograms, and the right-hand side scales refer to the unhatched histograms. Note that in all plots, the hatched bars lie typically to the right of the unhatched bars. The results of a comparison using the Kolmogorov–Smirnoff test are also shown in the diagrams. Submm point sources have been removed.

since these disproportionately affect the non-noise-weighted stacks. At both wavelengths, we then calculated the median noise levels in the unmasked regions, and then masked all areas with more than twice these noise levels. The 450-μm data quality is much more dependent on the weather conditions, so more of the 450-μm map is excluded by our noise cuts (e.g. Table 2). The results are shown in Figs 6 and 7. We detect the *Spitzer* galaxies at $\gg$ 99 per cent confidence at both 450 and 850 μm, and for all *Spitzer* wavelengths from 3–24 μm. We also detect the *ISO* 15-μm-selected population at 99.6 per cent confidence at 850 μm and 96 per cent confidence at 450 μm. The mean fluxes are given in Table 2, as are the Gaussian-equivalent σ values of the Kolmogorov–Smirnoff significance levels (though recall the uncertainties in the 450-μm flux calibration noted above). Our stacked mean fluxes are in good agreement with the previous determinations of Serjeant et al. (2004), though in addition we have made clear submm stacking detections at 3.6 and 4.5 μm. The mean flux ratios for the 5.8–8 μm selected galaxies presented in Table 2 are somewhat lower than those presented in Serjeant et al. (2004), which may be due to the lack of brighter *Spitzer* sources in the very small field of view of the Early Release Observations. There are some difficulties in interpreting these flux ratios, as they are summed from galaxies spanning a range of redshifts, and the contribution made by individual galaxies will depend on their location in the luminosity–redshift plane. Furthermore, the mean mid-IR flux is sensitive to the presence of the few brighter sources in the sample, which may lead to underestimates in the quoted errors in the flux ratios. We will return to this topic in Section 4. Another anomalous flux ratio is the 450:15 μm ratio; we believe this is due partly to small number statistics in this sample, and partly to the fact that only brighter mid-IR galaxies are detected at this wavelength which may bias the sample to submm-weak active galactic nucleus (AGN) dust tori. These galaxies are also only marginally detected (Table 2).

The Kolmogorov–Smirnoff test reports an apparently unrealistically small significance when comparing the 850-μm fluxes of 24-μm-selected galaxies with the submm map as a whole. Examination of the numbers in the bins of the histograms shows why this is the case; in effect, the probability that the distributions are identical is immeasurably small. To our knowledge, this is the best submm stacking detection ever made.

We constructed a noise weighted sum of the postage stamps around *Spitzer*/*ISO* galaxies selected at each wavelength. Figs 8 and 9 show the S/N images of the galaxies selected at these wavelengths. We clearly have strong detections of our sample at all wavelengths. Furthermore, the off-centre positions in these stacked postage stamps provide a control, and confirm the stacking is not prone to false positives. The weighted means are quoted in Table 2 and are in good agreement with the unweighted means. In particular, there is no evidence in Table 2 for weighted means systematically offset from the unweighted mean fluxes; any systematic offset must be far smaller than the random noise in the measurements.

Since our S/N is so high (unlike in the much smaller sample of Serjeant et al. 2004), we can investigate the subpopulations which dominate the stacking signal. In Fig. 10 we plot the comoving volume-averaged star formation rate (SFR) estimated from the

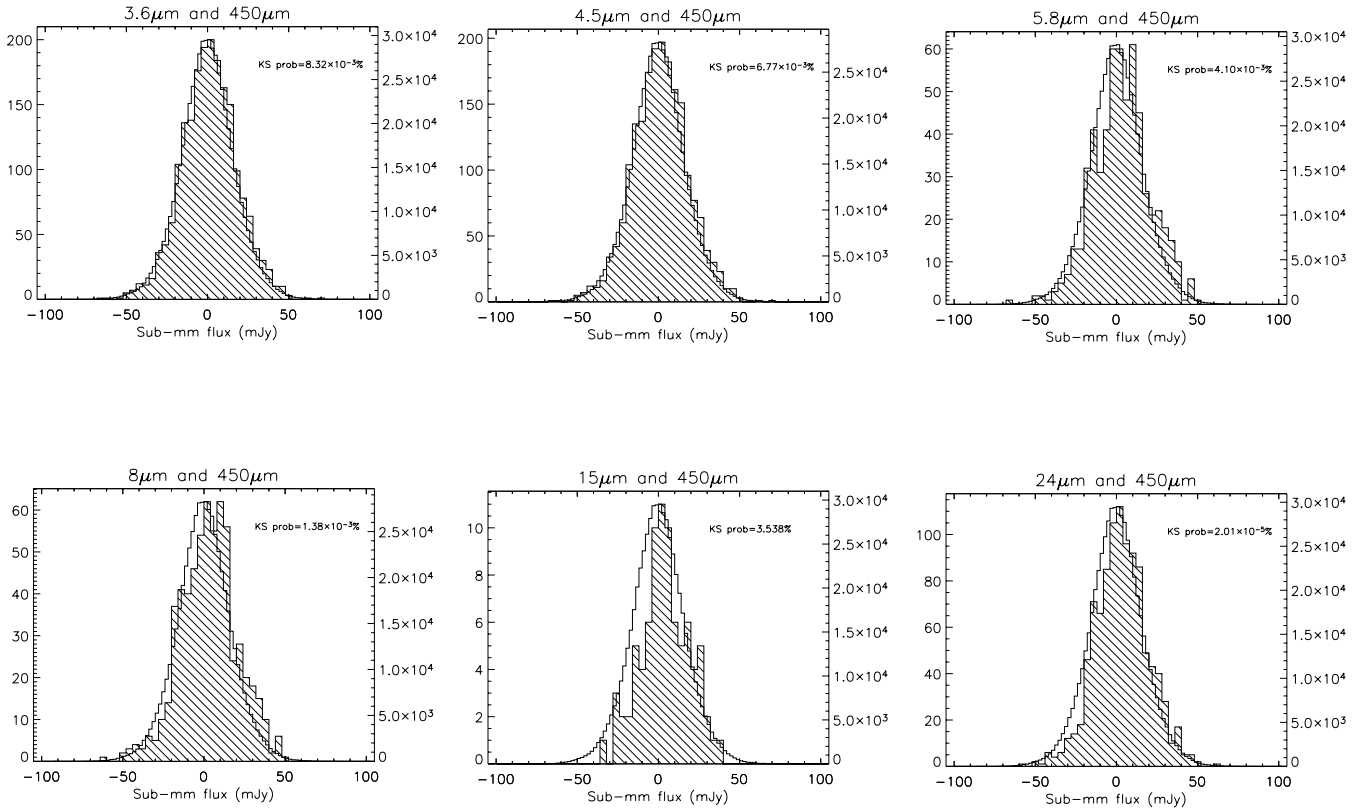

Figure 7. Histograms of 450-μm flux in the SHADES Lockman map as a whole (unhatched bars) compared to the 450-μm fluxes at the positions of the *Spitzer*/*ISO* galaxies selected at the indicated wavelengths (hatched bars). The left-hand side vertical scales show the numbers for the hatched histograms, and the right-hand side scales refer to the unhatched histograms. Note that in all plots, the hatched bars lie typically to the right of the unhatched bars. The results of a comparison using the Kolmogorov–Smirnoff test are also shown in the diagrams.

Table 2. Mean submm fluxes for *Spitzer*-selected and *ISO*-selected populations. Also quoted are the numbers of galaxies in each stacking analysis. Kolmogorov–Smirnoff significance values are quoted in Figs 6 and 7, and translated in this table into an equivalent number of σ of a Gaussian distribution as discussed in the text, except for the 850-μm detection of 24-μm sources which has a significance level too high for numerical inversion. The quoted errors on the mean fluxes are $\sigma/\sqrt{N}$, where N is the number of measurements and σ^2 the variance of the measurements, except in the case of flux ratios where the $\sigma/\sqrt{N}$ errors in each quantity have been propagated. Known submm sources have been subtracted from the maps prior to this analysis, as discussed in the text. The effect of the clustering of *Spitzer* galaxies is discussed in Section 3.6.

	3.6 μm	4.5 μm	5.8 μm	8 μm	15 μm	24 μm
N_{850}	4803	4676	1505	1558	188	2656
$\langle S_{850}\rangle$/mJy	0.184 ± 0.029	0.181 ± 0.029	0.302 ± 0.052	0.300 ± 0.051	0.43 ± 0.14	0.361 ± 0.041
$\langle S_{850}\rangle_{\rm weighted}$/mJy	0.195 ± 0.024	0.191 ± 0.024	0.318 ± 0.043	0.292 ± 0.042	0.54 ± 0.12	0.343 ± 0.033
$\langle S_{850}\rangle/\langle S_{\rm mid-}\ IR\rangle$	2.64 ± 0.24	3.49 ± 0.37	1.92 ± 0.27	2.80 ± 0.36	0.74 ± 0.08	1.98 ± 0.06
$\sigma_{\rm KS,850}$	5.3σ	5.9σ	4.6σ	5.3σ	2.6σ	$\gg 7\sigma$
N_{450}	1994	1977	586	625	84	1023
$\langle S_{450}\rangle$/mJy	1.23 ± 0.38	1.23 ± 0.39	2.98 ± 0.72	2.84 ± 0.70	4.1 ± 1.6	3.00 ± 0.51
$\langle S_{450}\rangle_{\rm weighted}$/mJy	1.55 ± 0.27	1.56 ± 0.27	3.00 ± 0.49	2.95 ± 0.47	3.6 ± 1.3	2.53 ± 0.36
$\langle S_{450}\rangle/\langle S_{\rm mid-}\ IR\rangle$	45.2 ± 5.1	72.6 ± 7.3	14.7 ± 3.8	30.0 ± 5.4	1.58 ± 0.2	11.5 ± 0.4
$\sigma_{\rm KS,450}$	3.8σ	3.8σ	3.9σ	4.2σ	1.8σ	5.1σ

850-μm stacked fluxes, assuming an M82 SED shape, and using a conversion derived for this SED from the Kennicutt (1998) conversion:

$$\frac{\rm SFR}{\rm M_\odot/year} = \frac{L_{\rm FIR}}{5.8\times10^9\,\rm L_\odot} = \frac{\nu L_\nu(60\,\mu\rm m)}{3.6\times10^9\,\rm L_\odot}. \quad (2)$$

This assumes a Salpeter initial mass function from 0.1 to 100 $\rm M_\odot$. Our estimator for the total submm flux contribution from a population of galaxies in a logarithmic mass interval $\Delta \log_{10} M$ is

$$F_{\rm tot}(\rm mJy\,deg^{-2}\,dex^{-1}) = \frac{1}{A\Delta\log_{10} M}\Sigma_{i=1}^{N} M(i)/c(i), \quad (3)$$

where A is the survey area, $M(i)$ is the submm map flux at the position of galaxy i (of which there are N) and $c(i)$ is the completeness of the *Spitzer* catalogue for galaxies similar to i. The calculation is not sensitive to the completeness correction. To first order both the submm and *Spitzer* fluxes are constant over the redshift intervals

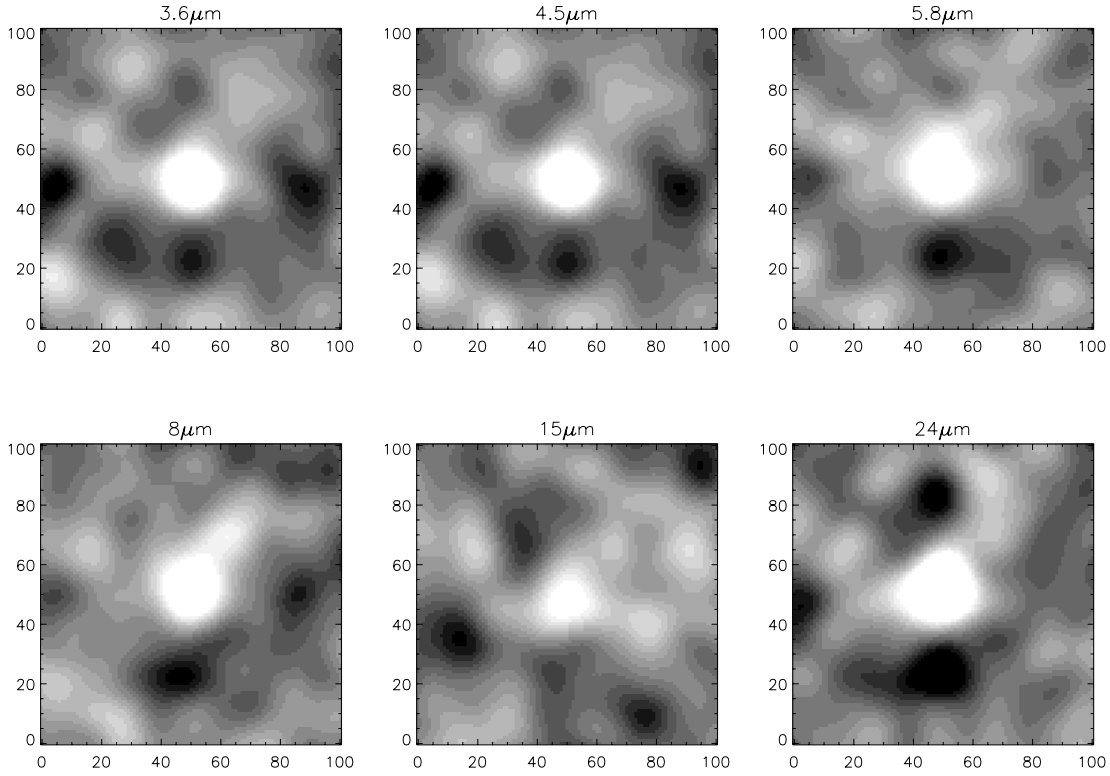

Figure 8. S/N images of stacked 850-μm postage stamps centred on *Spitzer*/*ISO* galaxies, as discussed in the text. The grey-scale is from -3σ to $+4\sigma$. The scales marked are arcseconds. Note the clear detections at the centres of all the images. Negative sidelobes are also visible.

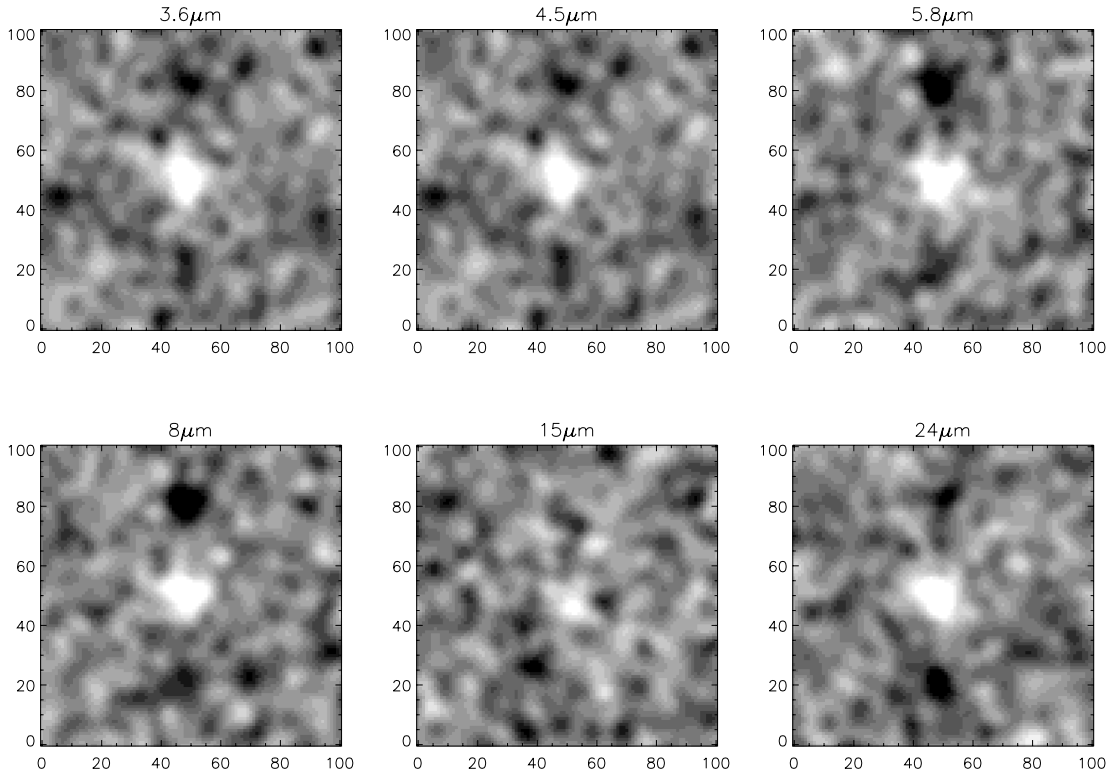

Figure 9. S/N images of stacked 450-μm postage stamps centred on *Spitzer*/*ISO* galaxies, as discussed in the text. The grey-scale is from -3σ to $+4\sigma$. The scales marked are arcseconds. Note the clear detections at the centres of all the images. Negative sidelobes are also visible.

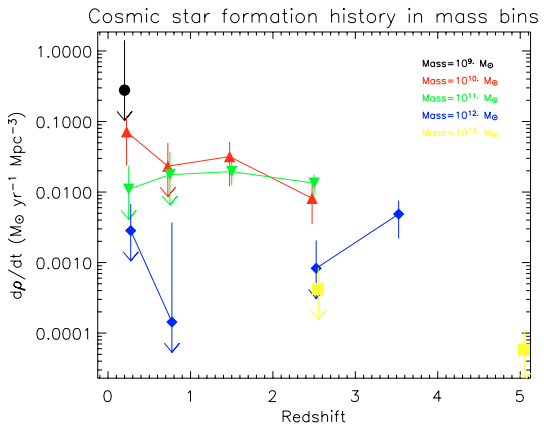

Figure 10. Evolution in comoving volume-averaged SFRs as a function of total mass for 3.6-μm-selected galaxies, in ±0.5 dex mass bins centred on the masses shown. The brighter submm point source population discovered by Smail, Ivison & Blain (1997), Barger et al. (1998) and Hughes et al. (1998) are not included, because we removed submm point sources prior to our stacking analysis. Symbols: the circle is $10^9\,M_\odot$, upward triangles $10^{10}\,M_\odot$, downward triangles $10^{11}\,M_\odot$, diamonds $10^{12}\,M_\odot$ and the square is the $10^{13}\,M_\odot$ constraint. Note that the lower mass galaxies have star formation histories peaking at much lower redshifts than the putative $z \simeq 2.2$ peak in the bright submm point source population.

in question (due to the negative *K*-corrections at both wavelength ranges). Our estimate of the error on the total flux is

$$\Delta F_{\rm tot} = \frac{1}{A\Delta \log_{10} M}\sqrt{\Sigma_{i=1}^{N}[M(i)/c(i)]^2}. \quad (4)$$

For conversion from 850-μm fluxes to luminosities, we use the central redshift of the bin, noting that the submm luminosity is roughly independent of redshift over the redshift ranges considered. We do not plot bins in which galaxies with masses equal to the mass at the centre of the bin are not above the *Spitzer* flux limit throughout the bin. We weight the flux contributions of each galaxy according to its accessible comoving volume. Fig. 11 shows the mean (quiescent) SFR per galaxy. Fig. 12 shows the mean (quiescent) SFR per unit galaxy mass, as a function of mass. This quantity has the dimensions of one over time (e.g. $\rm Gyr^{-1}$). This characteristic star formation time-scale can be regarded as the time-scale over which the bulk of the galaxy's baryonic matter would be converted into stars (though for consistency with elsewhere in this paper we use the total mass estimates for the galaxies, not just baryonic). The quantities plotted in Fig. 12 have no dependence on the completeness of the *Spitzer* catalogue, though the errors on the quantities depend on the sample size. We have also plotted the mass-doubling time-scale as a function of redshift on this figure, assuming $\rm SFR/\mathit{M}_*$ is constant; galaxies above this line may be regarded as starbursting. A further useful metric, also plotted in this figure, is the specific star formation required to build up the entire observed stellar mass since the big bang, assuming SFR is constant. For comparison, the specific SFRs of the SHADES point sources are shown in Fig. 13. We will discuss these figures in Section 4.2.

3.5 The cosmic near-IR and submm backgrounds

In Figs 14 and 15 we plot the contributions to the cosmic submm background light made by *Spitzer*/*ISO* galaxies, as a function of their near/mid-IR flux. We correct the *Spitzer*/*ISO* catalogues for incompleteness by comparison with published source counts from Fazio et al. (2004), Papovich et al. (2004) and Rodighiero et al. (2004). The figures show the submm background contribution per decade of near/mid-IR flux, and compare these contributions to those made by the same galaxies to the near/mid-IR backgrounds calculated from the published source counts.

There is a remarkably strong correspondence between the 24-μm-selected galaxy contribution to the 85-μm extragalactic background, and to the 24-μm-selected background. There is also a correspondence between the 3.6–4.5 μm selected galaxy contributions to the 450-μm extragalactic backgrounds, and to the 3.6–4.5 μm backgrounds. The 24-μm background contributions also correlate well with the 450-μm contributions. We will discuss the reasons for these correspondences in Section 4.

In Figs 16 and 17 we integrate the data in Figs 14 and 15, and plot the cumulative contributions to the cosmic submm background light, as a function of *Spitzer*/*ISO* flux. It is clear that about a quarter of the extragalactic 850-μm background light is resolved by *Spitzer*, and the majority of the 450-μm extragalactic background is resolved.

3.6 The impact of clustering on stacking analyses

Because of the limited resolution provided by SCUBA, we should be clear that the signal detected in the stacking analysis represents

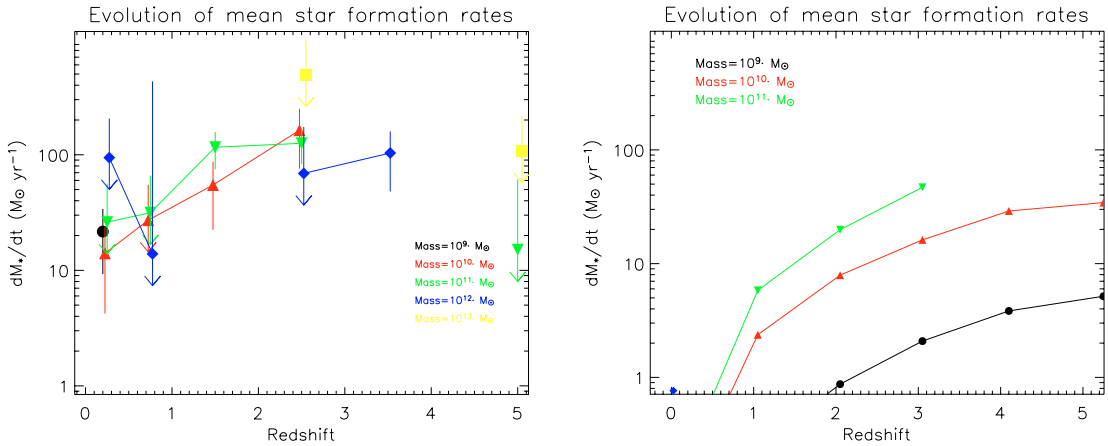

Figure 11. Left: mean SFRs, $\rm d\mathit{M}/dt$, of our galaxies. Symbols as in Fig. 10. Right: corresponding predictions from the de Lucia et al. (2006) simulation. Note that the observed SFRs clearly exceed the predictions.

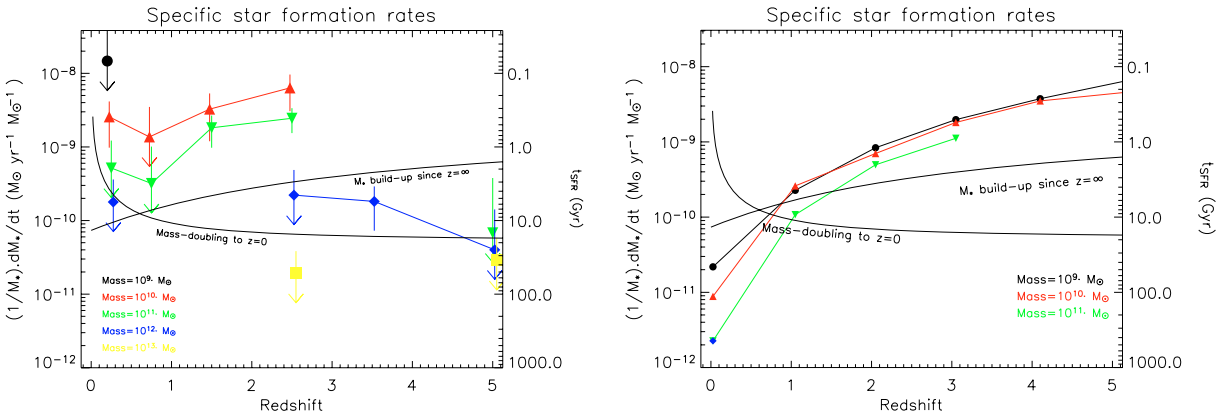

Figure 12. Left: SFR per unit galaxy mass, $(1/M)\,\mathrm{d}M/\mathrm{d}t$. This has dimensions of $[T]^{-1}$ and the corresponding star formation time-scales are given in the right-hand side ordinate. Symbols as in Fig. 10. Also plotted is the specific SFR required to double the stellar mass by $z = 0$ assuming a constant *specific* SFR, and the rate required to assemble the galaxy since the big bang assuming a constant SFR. Points lying above either line may be regarded as starbursting. Note that most of our detections can be regarded as starbursting. Right: corresponding predictions from the de Lucia et al. (2006) simulation. Note the obvious discrepancies with the observations.

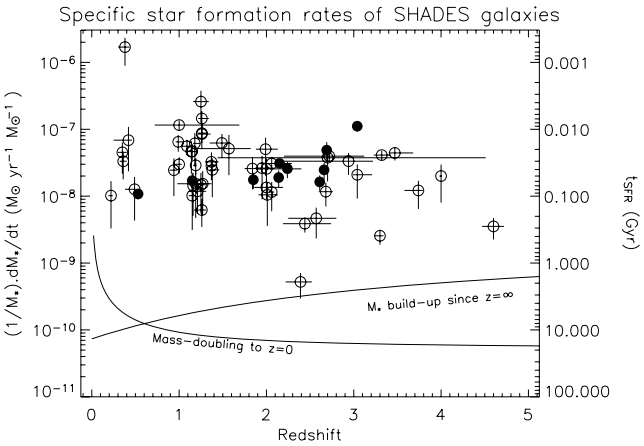

Figure 13. SFR per unit galaxy mass, $(1/M)\,\mathrm{d}M/\mathrm{d}t$, for the SHADES point sources in the Lockman Hole. As with Fig. 12, the corresponding star formation time-scales are given in the right-hand side ordinate. Objects with spectroscopic redshifts are shown in filled symbols, and objects with optical-*Spitzer*-based photometric redshifts from Dye et al. (2008) are shown as open symbols. Note that the star formation time-scales for SHADES sources are much shorter than in the population as a whole.

a contribution from any object within around 10 arcsec of the target *Spitzer*/*ISO* galaxies. Because these galaxies will be surrounded by a population of correlated neighbours, it is therefore possible that the stacked flux gives an overestimate of the emission from the target galaxies. This is simple enough to estimate: the additional flux is just the integral of the background intensity, I, times the angular cross-correlation between the target galaxies and the background, $w(\theta)$, times the beam B:

$$S = I \int w(\theta)\, B(\theta)\, 2\pi\theta\, \mathrm{d}\theta. \quad (5)$$

For a Gaussian beam, and assuming $w = (\theta/\theta_0)^{-0.8}$, this gives $S = 0.20(\theta_0/\mathrm{arcsec})^{0.8}$ mJy at 850 μm and $S = 0.28(\theta_0/\mathrm{arcsec})^{0.8}$ mJy at 450 μm. The appropriate value of θ_0 is of course open to debate, but Oliver et al. (2004) measure $\theta_0 = 1.24$ arcsec for the 3.6-μm-selected population. The stacked fluxes at 450 μm are at least five times the maximum value that could arise from neighbours (taking the extreme case in which all the 850-μm signal arises in this way). At 850 μm the contribution may be more significant, but the contribution estimated from equation (5) is necessarily an overestimate because not all the 850-μm background is attributable to these *Spitzer* galaxies. We can use Fig. 16, in which only ≃25 per cent of the 850-μm background is attributable to the *Spitzer* galaxies, to estimate iteratively the correlated 850-μm flux from the other *Spitzer* galaxies. This reduces the clustered contribution by a factor of 4, yielding $S = 0.06$ mJy with $\theta_0 = 1.24$ arcsec, which is at most a 20–30 per cent correction to the 850-μm fluxes quoted in Table 2. While non-zero, this is not sufficient to affect our conclusions.

4 DISCUSSION

4.1 The link between the near-IR and submm backgrounds

Any stacking analysis is only capable of determining the first moment of the distribution; the mean values in Figs 10 and 12 may belie a large variation in the population. We have also subtracted point sources, so strongly starbursting galaxies are omitted from these figures; we are therefore probing only the *mean quiescent* levels of star formation in these galaxies.

Our stacking detections have much higher S/N than any previously obtained, partly because of the depths of the *Spitzer* and SCUBA surveys, and partly also because the stacking S/N scales with the square root of the number of submm beams and SHADES has the largest contiguous submm survey fields to date. Our 450-μm stacking results are the best indicators of the populations that will be found to dominate the 450-μm background by SCUBA-2. The prospects are good for follow-ups of the ultradeep SCUBA-2 Cosmology Survey, because the *Spitzer* galaxies that appear to dominate the 450-μm background are less challenging targets for 8–10 m class spectroscopy than SCUBA point sources (e.g. Serjeant et al., in preparation). Similarly, the prospects appear good for spectroscopic follow-ups of ALMA point sources below the SCUBA-2 confusion limit. The clustering of bright submm point sources as a function of redshift is a key goal of the SHADES survey (e.g. van Kampen et al. 2005, Mortier et al. 2006), providing strong constraints on semi-analytic models of galaxy evolution; similarly, the

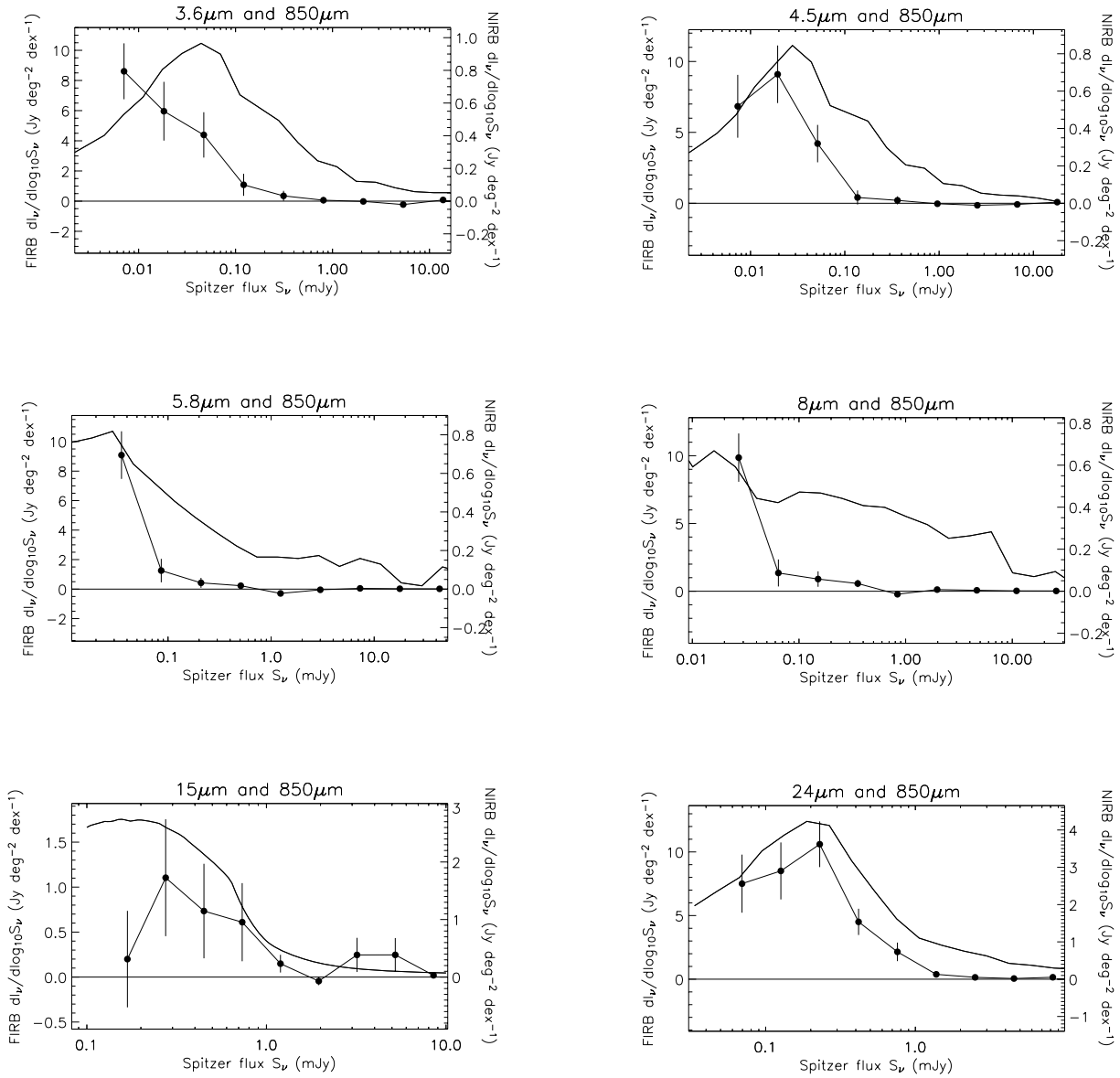

Figure 14. Contributions of the *Spitzer/ISO* galaxies to the 850-μm extragalactic background light (data points, left-hand side ordinates) as a function of *Spitzer/ISO* flux. Also plotted are the contributions of the same galaxies to the cosmic near-IR and mid-IR backgrounds (curves, right-hand side ordinates), estimated from the source counts as discussed in the text. Note in particular the correspondence between the 24- and 850-μm extragalactic backgrounds.

redshift-dependent clustering of galaxies a factor of ∼10 fainter in submm flux, for which optical follow-up is easier, is likely also to provide a strong constraint on such models.

Paradoxically, it is the brighter submm point sources that are the most challenging to follow up. The populations sampled by the SPIRE instrument on Herschel will be challenging to follow up in the optical (see also e.g. Khan et al. 2005, 2007). Spectroscopic redshifts for such populations may be better determined in the medium term by molecular line spectroscopy (e.g. Wagg et al. 2007), and in the longer term by SPICA (e.g. Nakagawa 2004).

We find that the submm:24 μm ratios for most 24-μm-selected galaxies are very different to those of most submm-selected galaxies, in agreement with Serjeant et al. (2004). If the 24-μm population had submm:24-μm flux ratios consistent with those of the submm point source population, the 24-μm sources considered in this paper would overproduce the 850-μm background by a factor of $\sim\times$ 3. We argue that the bulk of the *Spitzer* population has a quiescent star formation level much lower than that of submm point sources, while the latter are heavily obscured objects (e.g. Serjeant et al. 2003b; Clements et al. 2004; Smail et al. 2004) that are challenging for optical follow-ups, and far-IR 'loud' with high specific SFRs (Fig. 13) and short star formation time-scales. Such episodic star formation is supported by models of AGN feedback in massive galaxies in the early Universe, and by the small inferred mass accretion rates on to central supermassive black holes in submm point sources (e.g. Alexander et al. 2005).

The physical sizes of populations dominating the far-IR background are rather smaller than those inferred for submm point sources. At a flux density of ∼15 μJy, the 8-μm population which we have found to contribute significantly to the 450-μm extragalactic background has optical identifications in our imaging with typical diameters $\lesssim$ 1 arcsec (the optical identification diameters

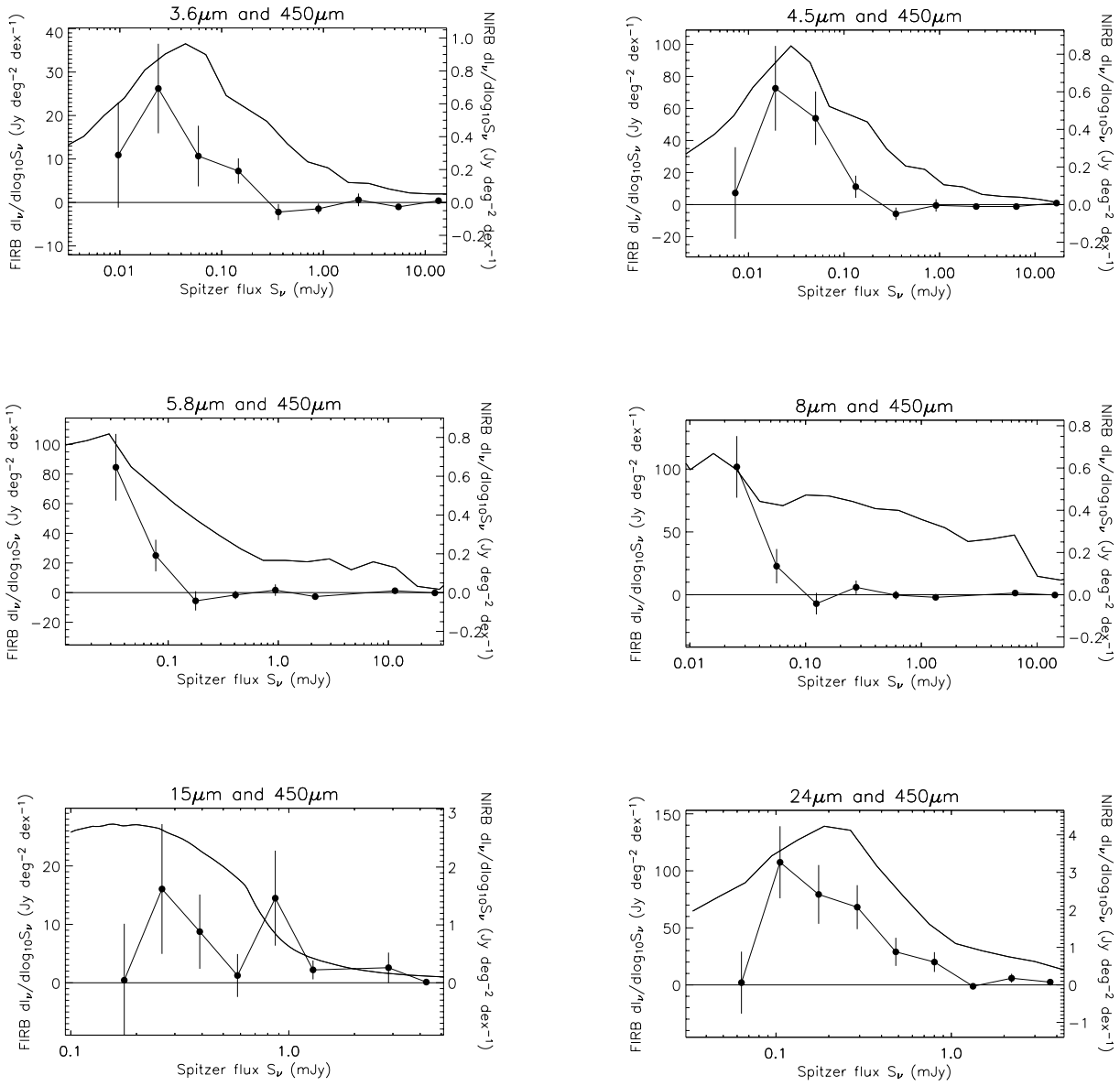

Figure 15. Contributions of the *Spitzer*/*ISO* galaxies to the 450-μm extragalactic background light (data points, left-hand side ordinates) as a function of *Spitzer*/*ISO* flux. Also plotted are the contributions of the same galaxies to the cosmic near-IR and mid-IR backgrounds (curves, right-hand side ordinates), estimated from the source counts as discussed in the text. Note in particular the correspondence between the 3.6–4.5- and 450-μm extragalactic backgrounds.

of submm point sources can be up to ∼2–4 arcsec, e.g. Smail et al. 2004; Pope et al. 2005, though other authors claim subarcsecond sizes, e.g. Chapman et al. 2004; Biggs & Ivison 2008). The regions of star formation in these galaxies will be resolvable with ALMA, which will probe the cool large-grained dust phase, and Darwin direct imaging which will probe the transiently heated small grains and PAH phases. This also suggests that 0.1 arcsec is the coarsest resolution that would be useful for a future ∼50–200 μm far-IR interferometer (FIRI) to resolve the internal structure of individual galaxies that comprise the cosmic far-IR background.

4.2 The mass dependence of star formation

When plotting the total contribution to the submm background from redshift shells in our *Spitzer* samples (not shown), we find that the $z \lesssim 1.5$ population is dominant, similar to the results of Wang et al. (2006). However, this neglects the fact that different luminosity and mass ranges are sampled at different redshifts. This may be one underlying cause of the difference between the Wang et al. (2006) and Dye et al. (2006) stacking results, since the *K*-correction effects are different in their respective samples; cosmic variance is another possibility. Ours is the first direct attempt to segregate the mass contributions to the submm-derived cosmic star formation history.

The mass segregation in Fig. 10 shows evidence for star formation in galaxies with model stellar masses $\simeq 10^{10}\,M_{\odot}$ assembling the bulk of their stellar masses at much lower redshifts than the estimated $z \sim 2.2$ peak in the submm point source population. This implies an increasing dominance at higher redshift of higher mass systems in the volume-averaged SFR. These observations are in accordance with qualitative expectations from 'downsizing' in star formation (Matteucci 1994; Bressan, Chiosi & Tantalo 1996; Cowie et al. 1996; see also Papers VII and VIII, Dye et al. 2008 and Clements et al. 2008, respectively).

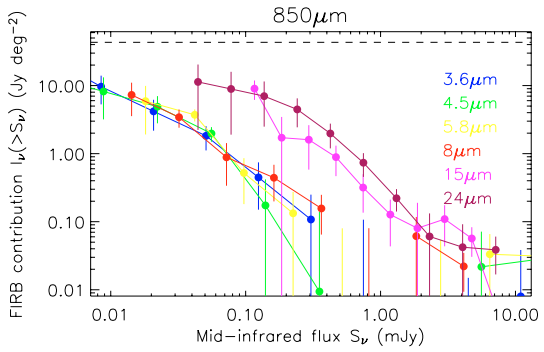

Figure 16. Cumulative contributions to the 850-μm extragalactic background light, as a function of near/mid-IR flux, for various *Spitzer/ISO* surveys. The horizontal dashed line is the total background derived by Lagache et al. (1999), the uncertainties on which are less than a factor of 2. Note that the *Spitzer* contributions converge to roughly a quarter of the total 850-μm background.

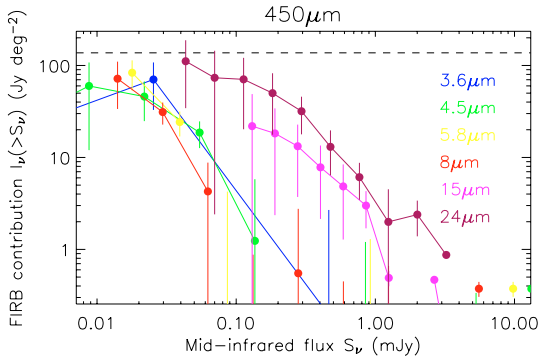

Figure 17. Cumulative contributions to the 450-μm extragalactic background light, as a function of near/mid-IR flux, for various *Spitzer/ISO* surveys. Symbols as Fig. 16. Note that the *Spitzer* contributions are capable of accounting for the entire 450-μm background, within the errors.

Fig. 11 shows the mass- and redshift dependence of the mean SFRs per *galaxy*, rather than per unit volume. The decrease in the mean SFRs per galaxy at $\sim 10^{10}\,M_\odot$ and $z < 1$ can only be reconciled with their increasing volume-averaged contribution if their number densities are increasing, in agreement with expectations from mass downsizing (e.g. Pozzetti et al. 2007). Fig. 11 also shows the corresponding predictions from the de Lucia (2005) Millenium Simulation. Our SFRs are a factor of a few higher than those predicted in this simulation.

The star formation time-scales in Fig. 12 at redshifts $z > 1$ scale approximately inversely with the mass of the system, quite unlike e.g. a Schmidt law for local late-type galaxies. In Fig. 12 we again compare this to the predictions from the de Lucia (2005) Millenium Simulations. Again, there is a striking discrepancy with the simulation predictions.

How bad would the photometric redshifts have to be in order to explain the disagreement between model and data? The results in Fig. 12 are surprisingly insensitive to photometric redshift, and it is therefore not likely that errors in the photometric redshifts are the cause of the disagreement. This insensitivity to redshift errors is due to the model stellar mass and SFRs both being relatively insensitive to redshift (e.g. Fig. 2) because both are to some degree subject to negative *K*-corrections. The specific SFR estimates therefore depend mainly on the submm:near-IR flux ratio, and not on redshift. It is

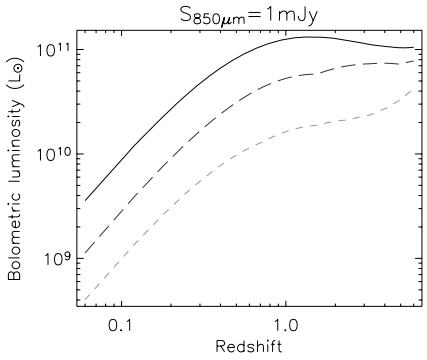

Figure 18. Bolometric luminosity as a function of redshift for an observed 850-μm flux of 1 mJy for three SEDs: M82 (full line), a cirrus-dominated spectrum from Efstathiou, Rowan-Robinson & Siebenmorgen (2000) (short dashed, green) and an Arp 220 model also from Efstathiou et al. (2000) (long dashed, green).

therefore hard to see how a redistribution of galaxies among the redshift bins could bring the data into agreement with the models; removing galaxies from one redshift bin to make it agree better with the models would make the disagreement worse in the other bins into which the galaxies are moved.

One hint that the SFRs may be overestimated comes from asking what will happen to the $10^{10}\,M_\odot$ galaxies if they continue forming stars at these high continuous rates. The galaxies appear to be forming stars at over 10 times the rate required to double their mass by the present day, almost regardless of redshift at $z < 2$. This is clearly not sustainable; it would require a rapid truncation of the star formation at slightly higher masses, and a continual feeding of lower mass galaxies into the $\sim 10^{10}\,M_\odot$ bin, for which there is no evidence in the stellar mass functions of galaxies (e.g. Bell et al. 2004, 2007; Caputi et al. 2006).

There are at least two possibilities that might reduce our estimates of the number of stars forming in these galaxies. One approach explored successfully by the Baugh et al. (2005) application of the Millenium Simulation is to assume a top-heavy initial mass function in star-forming galaxies. The reduction in the number of stars formed in this model is similar to the discrepancy between the de Lucia (2005) predictions and our measurements. However, the top-heavy initial mass function is normally only applied to extreme starbursting systems, and not to the quiescent star formation level in the galaxy population as a whole. A second possibility is that the observed-frame submm fluxes are dominated not by star formation, but by cool cirrus heated by the galaxies' interstellar radiation fields. The galaxies would then have a cooler SED than the M82 template assumed above. We demonstrate the strength of this effect in Fig. 18. Such a model was proposed for bright submm point sources by Efstathiou & Rowan-Robinson (2003) (see also Clements et al. 2008, Paper VIII), and although mm wave and radio interferometry have not on the whole yielded the large angular sizes predicted by these models (e.g. Tacconi et al. 2006; Ivison et al. 2007), it remains possible that these models are broadly correct descriptions of the fainter submm population.

4.3 The environment dependence of star formation

We have attempted to measure the matter environments of submm galaxies. Semi-analytic models predict that submm galaxies should be strongly clustered and lie in some of the largest overdensities at their redshifts (e.g. van Kampen et al. 2005), for which we have

found tentative evidence (e.g. Figs 4 and 5) and which agrees at least qualitatively with previous measurements (e.g. Blain et al. 2004; Blake et al. 2006). Recently, Elbaz et al. (2007) and Cooper et al. (2007) have shown evidence in the GOODS and DEEP2 surveys that $z \sim 1$ star-forming galaxies (as evidenced by 24-μm emission) are preferentially found in richer galaxy environments. This trend is in the opposite sense to that seen in the local Universe. Furthermore, the observed environment dependence of star formation is stronger than that predicted by semi-analytic models. Our observations extend this trend to higher redshifts and SFRs. The properties of the *star formation* density field, as opposed to the galaxy density field, may be a key arena for the future confrontation of data and semi-analytic predictions. Future Herschel and SCUBA-2 surveys will yield large catalogues of bright submm-selected galaxies, and their near-IR and submm environments will be easily measurable with the warm AKARI/*Spitzer* missions and SCUBA-2 follow-ups, respectively.

5 CONCLUSIONS

There is a strong correspondence between the galaxies that dominate the submm extragalactic background light and those that are detected in deep *Spitzer* surveys. The submm-derived specific SFRs in the *Spitzer* populations are much higher than those predicted by some semi-analytic simulations; this may be due to a component of submm emission heated by the interstellar radiation fields leading to overestimates of the SFRs, or to a top-heavy initial mass function in the *Spitzer* galaxies, or to some unknown deficiency in the models. We find evidence for downsizing in both star formation and mass assembly. We also find evidence that around a third of submm-selected galaxies at redshifts $1 < z < 1.5$ lie in the upper ∼20 percentile of the galaxy density distribution, in contrast to the redshift zero tendency of star-forming galaxies to avoid the richest environments.

ACKNOWLEDGMENTS

We would like to thank the referee, Wei-Hao Wang, for a careful reading of the manuscript and for helpful comments. SS would like to thank the Science and Technology Facilities Council for support under grants PP/D002400/1 and PP/D003083/1. KC and SD would like to thank the Science and Technology Facilities Council for support. IS acknowledges support from the Royal Society. AP acknowledges support provided by NASA through the *Spitzer* Space Telescope Fellowship Program, through a contract issued by the Jet Propulsion Laboratory, California Institute of Technology under a contract with NASA. Data were obtained at the JCMT under program M/02B/U52. The JCMT is operated by The Joint Astronomy Centre on behalf of the Science and Technology Facilities Council of the United Kingdom, the Netherlands Organisation for Scientific Research and the National Research Council of Canada. This work is based in part on observations made with the *Spitzer* Space Telescope, which is operated by the Jet Propulsion Laboratory, California Institute of Technology under a contract with NASA.

REFERENCES

Alexander D. et al., 2005, ApJ, 632, 736
Aretxaga I. et al., 2007, MNRAS, 379, 1571 (Paper IV)
Barger A. J. et al., 1998, Nat, 394, 248
Barger A. J., Cowie L. L., Sanders D. B., 1999, ApJ, 518, L5
Baugh C. M. et al., 2005, MNRAS, 356, 1191
Bell E. F. et al., 2004, ApJ, 608, 752
Bell E. F., Zeng X. Z., Papovich C., Borch A., Wolf C., Meisenheimer K., 2007, ApJ, 663, 834
Biggs A. D., Ivison R. J., 2008, MNRAS, 385, 893
Blain A. W., Kneib J.-P., Ivison R. J., Smail I., 1999, ApJ, 512, L87
Blain A. W., Chapman S. C., Smail I., Ivison R., 2004, ApJ, 611, 725
Blake C., Pope A., Scott D., Mobasher B., 2006, MNRAS, 368, 732
Bolzonella M., Miralles J.-M., Pelló R., 2000, A&A, 363, 476
Bressan A., Chiosi C., Tantalo R., 1996, A&A, 311, 425
Caputi K. I. et al., 2006, ApJ, 637, 727
Chapman S. C., Smail I., Windhorst R., Muxlow T., Ivison R. J., 2004, ApJ, 611, 732
Chapman S. C., Blain A. W., Smail I., Ivison R. J., 2005, ApJ, 622, 772
Clements D. et al., 2004, MNRAS, 351, 447
Clements D. et al., 2008, MNRAS, in press (Paper VIII)
Cooper M. C. et al., 2007, MNRAS, submitted (arXiv:0706.4089)
Coppin K. et al., 2006, MNRAS, 372, 1621 (Paper II)
Coppin K. et al., 2008, MNRAS, 384, 1597 (Paper VI)
Cowie L. L., Songaila A., Hu E. M., Cohen J. G., 1996, AJ, 112, 839
Cowie L. L., Barger A. J., Kneib J.-P., 2002, AJ, 123, 2197
de Lucia G., Springel V., White S. D. M., Croton D., Kauffmann G., 2006, MNRAS, 366, 499
Drory N. et al., 2004, ApJ, 608, 742
Dye S. et al., 2006, ApJ, 644, 769
Dye S. et al., 2008, MNRAS, in press (arXiv:0802.0497) (Paper VII)
Eales S. A. et al., 2000, AJ, 120, 2244
Efstathiou A., Rowan-Robinson M., 2003, MNRAS, 343, 322
Efstathiou A., Rowan-Robinson M., Siebenmorgen R., 2000, MNRAS, 313, 734
Elbaz D. et al., 1999, A&A, 351, L37
Elbaz D. et al., 2007, A&A, 468, 33
Fazio G. G. et al., 2004, ApJS, 154, 10
Ferreras I., Saha P., Williams L. L. R., 2005, MNRAS, 623, L5
Hughes D. H. et al., 1998, Nat, 394, 241
Ivison R. et al., 2007, MNRAS, 380, 199 (Paper III)
Kennicutt R. C., 1998, ApJ, 498, 541
Khan S. et al., 2005, ApJ, 631, L9
Khan S. et al., 2007, ApJ, 665, 973
Kovács A., Chapman S. C., Dowell C. D., Blain A. W., Ivison R. J., Smail I., Phillips T. G., 2006, ApJ, 650, 592
Lagache G., Abergel A., Boulanger F., Désert F. X., Puget J.-L., 1999, A&A, 344, 322
Lawrence A. et al., 2007, MNRAS, 379, 1599
Lonsdale C. et al., 2004, ApJS, 154, 54
Matteucci F., 1994, A&A, 288, 57
Mortier A. et al., 2005, MNRAS, 363, 563 (Paper I)
Nakagawa T., 2004, Adv. Space Res., 34, 645
Oliver S. et al., 2004, ApJS, 154, 30
Papovich C. et al., 2004, ApJS, 154, 70
Peacock J. A., 1999, Cosmological Physics. Cambridge Univ. Press, Cambridge
Peacock J. A. et al., 2000, MNRAS, 318, 535
Pope A. et al., 2005, MNRAS, 358, 149
Pope A. et al., 2006, MNRAS, 370, 1185
Pozzetti L. et al., 2007, A&A, 474, 443
Rieke G. et al., 2004, ApJS, 154, 25
Rodighiero G., Lari C., Fadda D., Franceschini A., Elbaz D., Cesarsky C., 2004, A&A, 427, 773
Scott S. E. et al., 2002, MNRAS, 331, 817
Scott S. E., Dunlop J. S., Serjeant S., 2006, MNRAS, 370, 1057
Serjeant S. et al., 2003a, MNRAS, 344, 887
Serjeant S. et al., 2003b, MNRAS, 346, L51
Serjeant S. et al., 2004, ApJS, 154, 118
Smail I., Ivison R. J., Blain A. W., 1997, ApJ, 490, L5
Smail I., Ivison R. J., Blain A. W., Kneib J.-P., 2002, MNRAS, 331, 495

Smail I., Chapman S. C., Blain A. W., Ivison R. J., 2004, ApJ, 616, 71
Tacconi L. J. et al., 2006, ApJ, 640, 228
Takagi T. et al., 2007, MNRAS, 381, 1154 (Paper V)
van Kampen E. et al., 2005, MNRAS, 359, 469
Wagg J. et al., 2007, MNRAS, 375, 745
Wang W.-H., Cowie L. L., Barger A. J., 2006, ApJ, 647, 74
Webb T. M. A., Brodwin M., Eales S., Lilly S. J., 2004, ApJ, 605, 645

This paper has been typeset from a TEX/LATEX file prepared by the author.